

The role of the microscale contact line dynamics in the wetting behaviour of complex fluids

D. BIOLE`E, V. BERTOLA

*School of Engineering
University of Liverpool
Brownlow Hill, Liverpool L69 2GH, UK
e-mail: Volfangio.Bertola@liverpool.ac.uk*

THE MICROSCALE MORPHOLOGY OF THE LIQUID-SUBSTRATE CONTACT LINE is studied experimentally in two well-known examples of dynamic wetting with complex fluids (namely, drop impact of dilute polymer solutions and spreading of superspreader surfactant solutions). High-speed, high-magnification images of the contact line details were obtained using a high-frame rate camera equipped with a digital microscope zoom lens. Unlike in the case of simple liquids, which exhibit a smooth contact line, the advancing or receding contact line of complex fluids shows peculiar transient features which extend significantly in the radial direction (perpendicular to the contact line itself). It is argued such microscopic features determine the macroscopic dynamic wetting behaviour of complex fluids.

Key words: dynamic wetting, contact line, dilute polymer solutions, superspreaders.

Copyright © 2015 by IPPT PAN

1. Introduction

THE INTERACTION OF A LIQUID DROP with a solid surface is a classic problem [1], which underpins our understanding of several wetting and de-wetting processes in practical applications, including coating and thin film deposition processes, sprays, bio and microfluidics. In typical applications, the drop size ranges from a few μm (aerosols) to a few mm (agricultural sprays), with corresponding liquid volumes ranging from femtolitres to microlitres. The equilibrium shape of a drop deposited on a surface is generally described using the well-known Young-Laplace equation with respect to the interfacial tensions between the solid and the liquid γ_{SL} , the solid and the vapour γ_{SV} , and the liquid and the vapour γ :

$$(1.1) \quad \gamma_{\text{SL}} + \gamma \cos \theta_{\text{eq}} = \gamma_{\text{SV}},$$

where θ_{eq} is the thermodynamic equilibrium contact angle between the drop and the surface [2].

If the drop moves parallel to the surface, one can however observe an advancing (θ_A) and a receding contact angle (θ_R), respectively at the leading edge and at the trailing edge. This implies an additional component in the Young–Laplace force balance, which can be described either by using Furmidge’s equation [3, 4]:

$$(1.2) \quad F = \gamma D(\cos \theta_R - \cos \theta_A),$$

where D is the drop base diameter perpendicular to the contact angle plane, or by introducing the concept of line tension for systems featuring significant contact line pinning and contact angle hysteresis [5]:

$$(1.3) \quad T = \gamma \frac{D}{2}(\cos \theta - \cos \theta_{\text{eq}}),$$

where θ is the apparent (observed) contact angle. A comparative analysis of these two approaches can be found in [6]. Different approaches must be used in case of chemically heterogeneous [7, 8] or rough surfaces [9, 10], and in case of non-circular drops [11].

Whilst the above theories are relative to drops of pure liquids deposited on perfectly smooth homogeneous surfaces, many applications involve the use of complex fluids, such as polymer or surfactant solutions, which exhibit a wetting dynamics remarkably different from the case of simple liquids. Even in the case of very dilute solutions, comparison with the Newtonian solvent (e.g., water) reveals significant differences in the behaviour of the moving contact line during the spreading and/or receding phase, in the amplitude of the dynamic contact angle, as well as in the intrinsic time of the phenomenon [12].

A well-known example is the so-called anti-rebound effect of polymer additives, illustrated in Fig. 1. When a droplet of water falls onto a hydrophobic surface, such as the waxy leaf of a plant, the drop is often observed to bounce off. However, for about 15 years it has been known that the addition of very small quantities (~ 100 ppm) of a flexible polymer such as polyethylene oxide (PEO) can completely prevent rebound, by reducing the recoil velocity of the drop after the inertial spreading of two orders of magnitude [12,13]. This is surprising since the shear viscosity and surface tension of such drops are almost identical to those of pure water [14]. Early attempts to explain this phenomenon in terms of the bulk rheology of the fluid [14, 15], or invoking normal stresses [16], turned out to be severely flawed, mainly due to glaring selective manipulations and/or misinterpretation of experimental data used in support of these approaches, as discussed in detail in [12], which surprisingly were not flagged during the peer-review process.

Another outstanding example of dynamic wetting with a complex fluid is so-called superspreading (or superwetting), a fascinating phenomenon observed with dilute solutions of certain trisiloxane surfactants on hydrophobic substrates

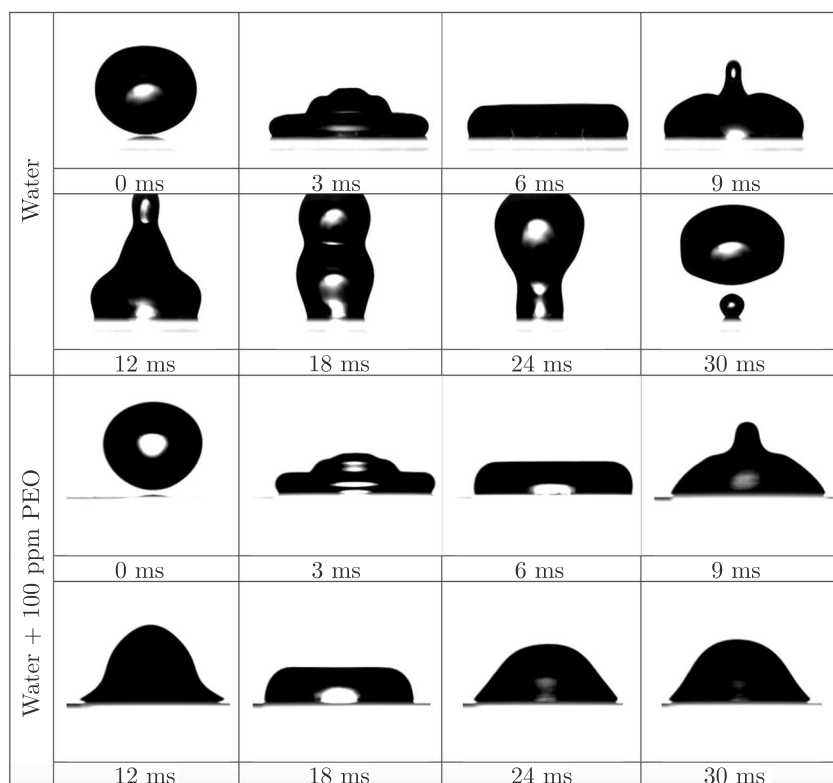


FIG. 1. Impact of water (top) and 200 ppm polymer solution (bottom) drops ($D_0 \sim 3\text{mm}$) impacting on a PTFE surface (release height: 20 mm).

(see [17], and references therein). As shown in Fig. 2, a liquid droplet containing as low as 0.1% of a superspreading surfactant can wet out on a hydrophobic surface, covering an area 100 times larger than a water droplet.

Although the physicochemical mechanisms at the origin of these phenomena are completely different from each other, in both cases they affect the morphology

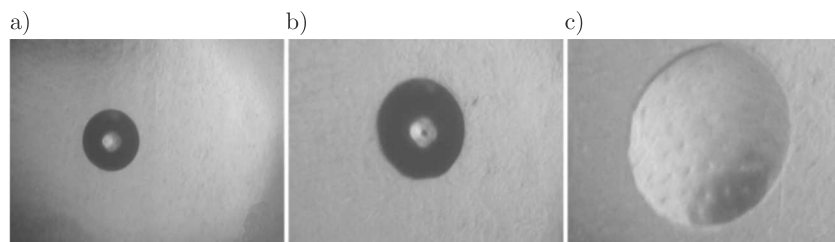


FIG. 2. Spreading of a liquid droplet on a polypropylene surface, 300 s after deposition: a) water drop, b) 0.1% aqueous solution of Break-Thru S233 surfactant (non-superspreader), c) 0.1% aqueous solution of Break-Thru S240 surfactant (superspreader).

of the advancing or receding contact line at the microscopic level. This paper presents an experimental study of the microscale contact line morphology of complex fluid droplets interacting with a solid substrate, showing how it can be related to the macroscopic dynamic wetting behaviour. In particular, the paper focuses on the two examples mentioned above (impact of dilute polymer solutions and spreading of superspreader surfactant solutions, both on hydrophobic substrates). In the case of dilute polymer solutions (anti-rebound effect), high-magnification images reveal that, as opposed to pure water, the contact line of dilute polymer solutions is pinned at several points on the impacting surface, and the polymer solution forms liquid filaments on the substrate. In the case of superspreading, one can observe the formation of microscopic fingers at certain preferred positions along the contact line.

2. Materials and methods

2.1. Fluid preparation and characterisation

The fluids used in the present study were aqueous solutions of a high-molecular weight flexible polymer, polyethylene oxide (Sigma-Aldrich) and two different trisiloxane surfactants, known with the commercial names of Break-Thru S233 and S240, respectively (Evonik). Both chemicals were dissolved in deionised water (Barnstead Easypure).

Polyethylene oxide (PEO) was supplied in powder form, with average molecular weight of 4000 kDa. Dilute solutions with different weight concentrations (400 ppm, 300 ppm, 200 ppm, 100 ppm, 60 ppm, and 40 ppm) were obtained by successive dilution of a master solution. In dilute solutions, the average distance among polymer molecules is larger than their characteristic size, so that their interactions are negligible: polymers exhibit a random coil conformation and can be described as spherical particles suspended in the solvent. For a critical value of concentration (the overlap concentration) polymer chains become randomly entangled, which corresponds to a marked increase in the polymer solution viscosity. The overlap concentration can be calculated as

$$(2.1) \quad c^* = \frac{1}{[\eta]},$$

where $[\eta]$ is the characteristic viscosity, which for a PEO solution in water ($T \approx 22^\circ\text{C}$) is related to the molecular weight, M_w , as [18]:

$$(2.2) \quad [\eta] = 0.0125M_w^{0.178}.$$

Thus, for the solutions considered in the present work the overlap concentration is $c^* = 567$ ppm.

Viscosities were measured by means of a capillary viscometer (Aldrich Chemistry, diameter 50 μm), while equilibrium surface tensions were measured using a maximum bubble pressure instrument (Krüss PocketDyne). Finally, the relaxation time was calculated as a function of the characteristic viscosity, concentration and temperature using the empirical formula [19]:

$$(2.3) \quad \tau = \sqrt{c}(1.82 \times 10^{-3}[\eta]_0 - 2.9 \times 10^{11}[\eta]_0^3 - 0.51) \exp(-0.0004T^2).$$

In dilute regime, viscosity η and the relaxation time τ are approximately a linear and a square root function of the polymer concentration, respectively, as shown in Fig. 3. Unlike η and τ , the surface tension σ of PEO solutions is approximately the same as the solvent (~ 70 mN/m) on the timescale of experiments [20], because PEO saturates the free surface already at low concentrations; similarly, the density variation is negligible with respect to the density of the solvent.

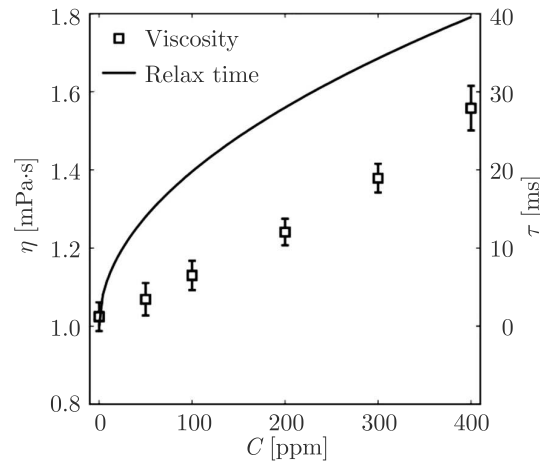


FIG. 3. Viscosity and relaxation time of dilute PEO solutions as a function of the polymer concentration. The error bars represent the standard deviation of a set of 10 measurements.

Surfactant solutions with a weight concentration of 0.1% were obtained by dissolving surfactants S233 and S240, both supplied as a liquid; the resulting equilibrium surface tension of the solutions was 23 mN/m and 22 mN/m, respectively. To investigate superspreading independently of the system properties, the two surfactants have similar chemical structure, but only one, S240, is a superspreader.

2.2. Experimental apparatus

The schematic of the experimental setup is displayed in Fig. 4. Drops were released from a blunt hypodermic needle (gauge 21, internal diameter 0.5 mm)

suspended above the target substrates. The equilibrium diameter, calculated from drop weight measurements ($D_0 = \sqrt[3]{6m/\pi\rho}$) was 2.8 mm for polymer solution drops and 2 mm for surfactant solution drops. In all cases the drop equilibrium radius $D_0/2$ was smaller than the capillary length $a = \sqrt{\sigma/\rho g}$, (2.4 mm for polymer solutions and 1.5 mm for surfactant solutions), which is indicative of the competition between surface forces and gravity; this means surface forces prevail ensuring a spherical equilibrium shape of drops.

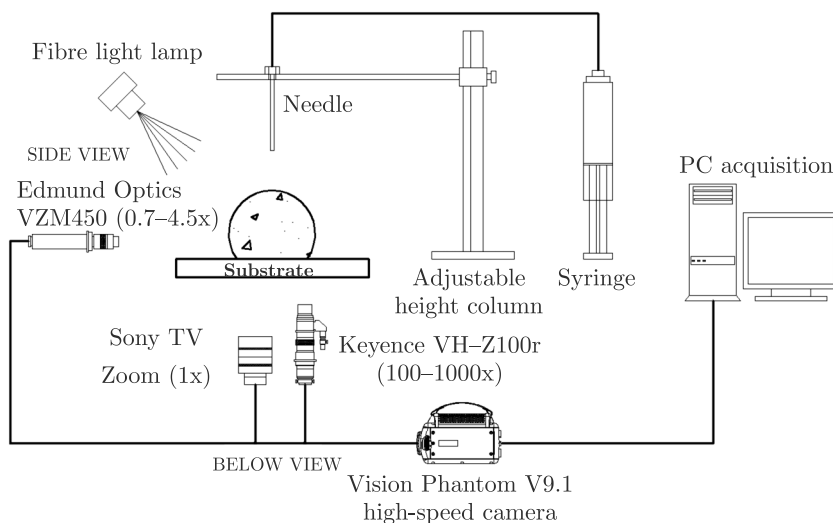


FIG. 4. Schematic of the experimental setup.

While surfactant solution drops were gently deposited on the substrate, polymer solution drops were released from different heights (20 mm, 60 mm, 100 mm and 140 mm, respectively) to change the impact velocity, calculated as the theoretical free fall velocity $u = \sqrt{2g(H_F - D_0)}$; a previous study showed this is almost identical to the measured impact velocity, for falling heights up to 30 cm [21]. Drop impacts were characterized through the Weber number, $We = \rho u^2 D_0 / \sigma = 2\rho g D_0 (H_F - D_0) / \sigma$, expressing the balance of inertia and surface forces; in particular, with average impact velocities of 0.58 m/s, 1.06 m/s, 1.38 m/s and 1.64 m/s, the Weber numbers of the present experiments were 13, 45, 76 and 107.

The substrates used for polymer solution drops were glass slides coated with Fluoropel PFC1302A (Cytonix Corp.), a 2% fluoropolymer solution in low boiling point (135°C) fluorosolvent, with equilibrium contact angle for water of $105 \pm 2^\circ$; the Fluoropel coating was created by dipping glass slides into the liquid, and then dried at 90°C for 10 minutes to optimize adhesion. Surfactant solution drops were deposited on a commercial transparent polycarbonate substrate, with equilibrium contact angle for water of $54 \pm 2^\circ$.

The contact line details during drop impact and recoil (in the case of polymer solutions) and during capillary spreading (in the case of surfactant solutions) were recorded using a high-speed CMOS camera (Phantom v9.1) equipped with a Keyence VH-100ZR zoom lens (magnification range of 100x–1000x), at the speed of 5000 frames per second (FPS) and a resolution of 576×576 pixels; the camera and the lens were arranged vertically looking at the substrate from beneath, as shown in Fig. 4. Illumination was provided by a fiber optic halogen illuminator (ThorLabs). For each set of experimental parameters, the experiment was repeated five times for the sake of statistical analysis.

2.3. Procedure

High-speed movies were processed frame-by-frame using a Matlab® application to highlight the contact line and its features. Raw images were first converted to binary images through an algorithm that included background removal, noise reduction (holes filling in the case of dark pixels noise, morphological erosion in the case of bright pixels noise), and finally contour line cleanup from neighbouring pixels artificially connected to pixels on the contour line (i.e., those pixels connected to the line by a bridge with pixel intensity smaller than a given threshold value).

3. Results

3.1. Receding contact line of dilute polymer solution drops

A typical drop impact process such as the one displayed in Fig. 1 involves an inertial spreading stage, where the impact kinetic energy is partly stored as surface energy and partly dissipated; after the drop has reached maximum spreading, one can observe a retraction stage, driven by capillary forces that tend to restore the spherical shape of the drop in order to minimize surface energy [22]. While during the inertia-dominated spreading stage the advancing contact angles observed for water and dilute polymer solutions are identical, during the capillary-driven retraction stage the receding contact angle observed in case of dilute polymer solutions is significantly smaller than that of water drops [12, 23]. This corresponds to a substantial reduction (two orders of magnitude) of the contact line receding velocity [12, 13], which in turn prevents dilute polymer solution drops from bouncing off hydrophobic surfaces.

The microscale analysis of the contact line morphology provides a key to understanding the peculiar behaviour of polymer solution drops as compared with water drops. Figure 5 displays magnified images of a short arc of the contact line at different times during drop retraction, for a dilute polymer solution drop and for a water drop with the same diameter impacting on the same surface with

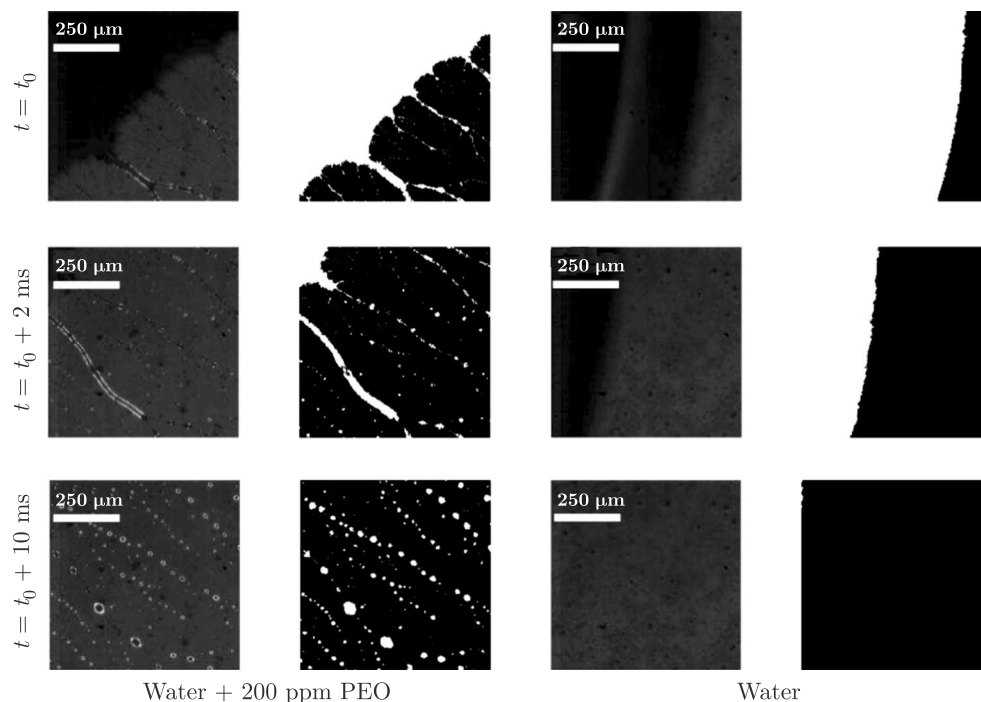


FIG. 5. Comparison between the contact line details of a dilute polymer solution drop (left) and a water drop (right) during the retraction stage after impact on a hydrophobic surface.

the same impact velocity. While the contact line of the water appears almost perfectly smooth, the contact line of the polymer solution drop exhibits large local deformations, and leaves behind microscopic liquid filaments as it sweeps the surface. Filaments are distributed uniformly around the contact line, and are likely to originate in points of localized pinning. The size of these filaments, which is approximately $10\ \mu\text{m}$ in width, decreases in time (the filaments tend to become thinner and disappear), until the fluid locally breaks up into secondary microscopic droplets, similar to the well-known bead-on-a-string breakup mechanism characteristic of many viscoelastic fluids. Furthermore, the complexity of these filaments, in terms of spatial displacement, orientation and size, grows both with the impact speed and with the polymer concentration in the fluid; in fact, reducing the polymer concentration from 200 ppm to 40 ppm the liquid filaments become less noticeable ($2\ \mu\text{m}$ width), and disappear when the impact speed is lower than 1 m/s. The mean diameter of the secondary droplets formed after the liquid filaments have broken up is $5\text{--}15\ \mu\text{m}$ in the case of 200 ppm polymer solution impacting with velocity of 1.64 m/s, but tends to smaller values for decreasing impact velocities and polymer concentrations.

As the contact line moves, and before breaking up into smaller beads, the filaments generate dendritic structures rooted on the contact line itself and extending on the outer surface. Such complex morphology observed at the microscale suggests that, even from the macroscopic point of view, the terminology “contact line” is not appropriate to indicate the drop edge, but one should rather use the expression “apparent contact line”. Figure 5 also demonstrates the importance of image processing in the identification of the thinner filaments and the smaller beads, which could hardly be observed in raw images.

It is well known that dilute solutions of flexible polymers in uniaxial elongational flow, which occurs for example in a stretched liquid filament, exhibit a non-zero normal stress difference, resulting into a net tensile force in the direction of stretching:

$$(3.1) \quad F_T = \frac{\pi d^2}{4} \left(\tau_{zz} + \frac{4\gamma}{d} \right),$$

where d is the filament diameter and τ_{zz} the normal stress component in the direction of stretching, which in simple cases (e.g., constant elongation rate) can be calculated analytically using the FENE-P constitutive equation [24]. Adding up the tensile forces of filaments distributed along one half of the contact line, projected in one direction, as shown schematically in Fig. 6, yields a net positive contribution to the line tension defined in Eq. (3.1) above:

$$(3.2) \quad 2T = \sum_{i=1}^N F_T^i \cos(F_T^i \hat{O}x),$$

where T is the filaments contribution to the line tension, N is the number of active filaments distributed along one half of the contact line, F_T^i is the tensile

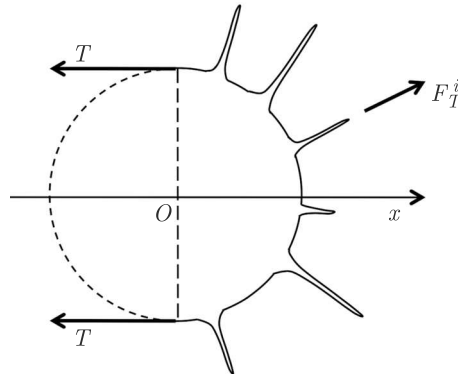


FIG. 6. Schematic of the force balance on the apparent contact line of a dilute polymer solution drop, retracting after impact on a hydrophobic surface.

force in the i -th filament, and $F_T^i \hat{O}x$ the angle formed by the i -th filament and a fixed direction. According to Eq. (3.1)), increasing the line tension implies a reduction of the apparent contact angle, which is in agreement with experimental observations [12, 23].

3.2. Advancing contact line of superspreader surfactant solutions

Drops of surfactant solutions were gently deposited on the substrate; thus, inertia is negligible and one can only observe liquid spreading driven by capillary forces. Unlike water droplets, which attain equilibrium almost immediately, superspreader surfactant solutions are known to wet out on moderately hydrophobic surfaces, such as the one used in the present experiments. However, the physico-chemical mechanism of this phenomenon is poorly understood to date [17]. The analysis of available literature data suggests it occurs when solutions of particular trisiloxane surfactants spread on certain substrates characterized by a moderate hydrophobicity, with equilibrium contact angles for pure water around 50° .

When the advancing contact line of a superspreader surfactant solution drop is observed at the microscale, one can clearly visualise the formation of microscopic fingers at certain preferred positions along the contact line, as shown in Fig. 7. These fingers rapidly develop into semi-dendritic structures, which pull the liquid in the droplet beyond the contact line and therefore enhance spreading. This peculiar morphology cannot be observed in the case of non-superspreader trisiloxane surfactant solutions, which exhibit a generally smooth contact line.

Although the dendritic structures observed for superspreader surfactant solutions are morphologically different from those observed for dilute polymer solutions, they seem to have a similar effect on the contact line dynamics, i.e., they change the line tension by applying a force directed from the liquid side of the apparent contact line outwards. In the case of dilute polymer solution drops recoil, this force is opposed to the contact line movement, therefore it causes a deceleration, whereas in the case of surfactant solution drops spreading it has the same direction, therefore it causes an acceleration.

This is further confirmed by the analysis of the equivalent base diameter of surfactant solution drops, defined as $D = \sqrt{4A/\pi}$, where A is the wetted area, displayed as a function of time in Fig. 8. Immediately after the drop deposition, the non-superspreader surfactant (S233) solution wetted area grows at a faster rate than the superspreader surfactant (S240) solution; however, once the contact line protrusions start growing on the contact line, this trend is reversed, and the wetted area of the superspreader surfactant grows more than that of the non-superspreader surfactant. For the sake of comparison, Fig. 8 also displays the equivalent diameter of a water drop, which remains constant as expected.

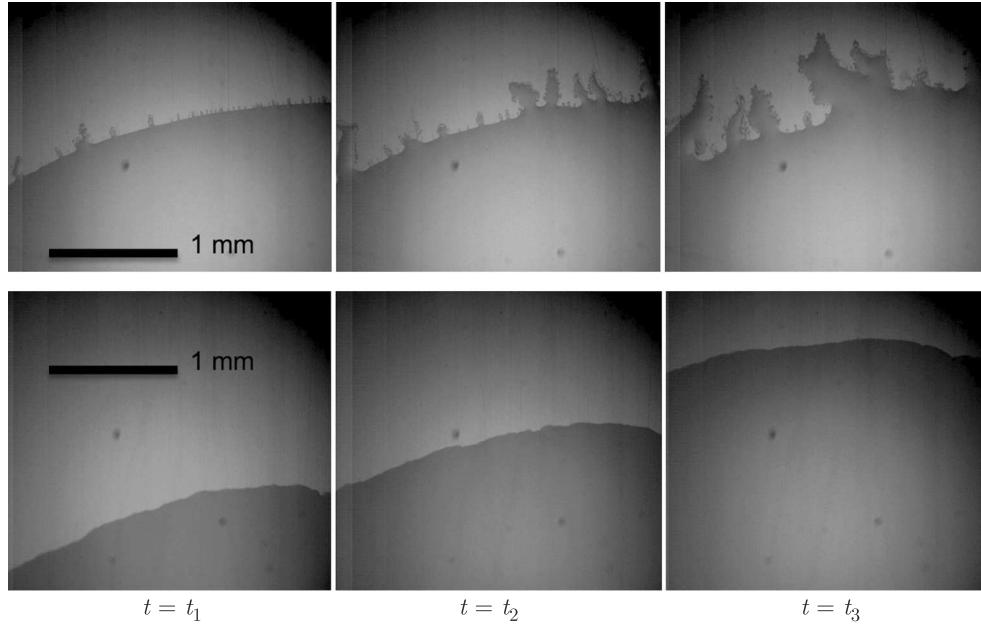


FIG. 7. Contact line detail of two 0.1% trisiloxane surfactant solution drops during spreading on a polycarbonate surface, at different times ($t_3 > t_2 > t_1$). Top: superspreader surfactant solution (Break-Thru S240), bottom: non-superspreader surfactant solution (Break-Thru S233).

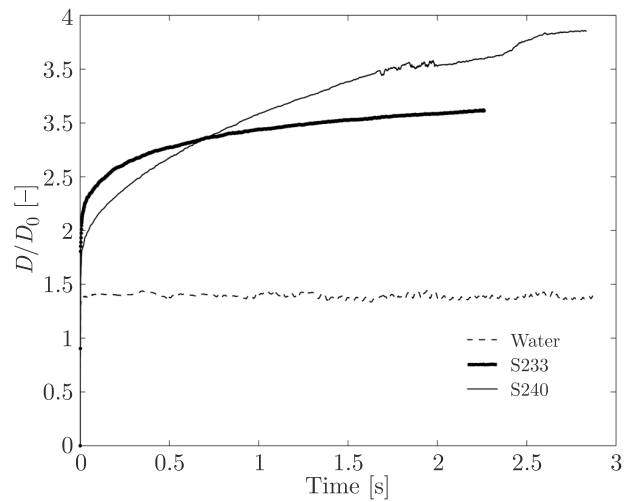


FIG. 8. Dimensionless equivalent diameter of three liquid droplets spreading on a polycarbonate surface; superspreader surfactant solution (thin line), non-superspreader surfactant solution (thick line), and water (broken line).

It must be remarked that while in the case of dilute polymer solutions one can understand the contribution to the line tension of liquid filaments stemming out of the apparent contact line in terms of the non-Newtonian constitutive equation of the fluid, the physico-chemical mechanism originating the microscopic structures observed during the spreading of surfactant solutions, as well as their effect on the contact line tension, remains unknown.

4. Conclusions

The microscale morphology of the advancing or receding contact line of a liquid drop on a solid surface plays a fundamental role in determining the wetting or de-wetting dynamics of complex fluids observed from the macroscopic standpoint. Experimental evidence is provided by two examples: the impact of dilute polymer solution drops on hydrophobic surfaces and the capillary spreading of superspreader surfactant solutions on a moderately hydrophobic surface. In particular, in the case of dilute polymer solutions one can observe filament-like microstructures distributed along the apparent contact line, which reduce significantly the contact line velocity during the retraction stage after maximum spreading; in the case of superspreader surfactant solutions, microscopic liquid protrusions were observed during capillary spreading, which are believed to enhance the spreading factor of these fluids.

Whilst the effect of the contact line morphology on the de-wetting behaviour of dilute polymer solutions can be understood in terms of the non-Newtonian constitutive equation of the fluid, the mechanism underlying the spreading enhancement observed in superspreader surfactant solutions remains unknown.

Acknowledgment

This work was supported by the University of Liverpool – A*STAR (Singapore) partnership.

References

1. P-G. DE GENNES, *Wetting: statics and dynamics*, Reviews of Modern Physics, **57**, 827–863, 1985.
2. T. YOUNG, *An essay on the cohesion of fluids*, Philosophical Transactions of the Royal Society of London, **95**, 65, 1805.
3. C.G.L. FURMIDGE, *Studies at phase interfaces. I. The sliding of liquid drops on solid surfaces and a theory for spray retention*, Journal of Colloid Science, **17**, 309–324, 1962.

4. E.B. DUSSAN, *On the ability of drops or bubbles to stick to non-horizontal surfaces of solids. Part 2. Small drops or bubbles having contact angles of arbitrary size*, Journal of Fluid Mechanics, **151**, 1–20, 1985.
5. J.W. GIBBS, *On the equilibrium of heterogeneous substances*, Transactions of the Connecticut Academy of Arts and Sciences, 1876.
6. R. TADMOR, *Approaches in wetting phenomena*, Soft Matter, **7**, 1577–1580, 2011.
7. A. FRIEDMAN, *Wetting and adsorption at chemically heterogeneous surfaces*, [in:] Mathematics in Industrial Problems, The IMA Volumes in Mathematics and its Applications, **57**, 185–197, Springer, New York, 1994.
8. P.S. SWAIN, R. LIPOWSKY, *Contact angles on heterogeneous surfaces: A new look at Cassie's and Wenzel's laws*, Langmuir, **14**, 6772–6780, 1998.
9. E. BORMASHENKO, *Wetting transitions on biomimetic surfaces*, Philosophical Transactions of the Royal Society A, **368**, 4695–4711, 2010.
10. E. BORMASHENKO, Y. BORMASHENKO, G. OLEG, *On the nature of the friction between nonstick droplets and solid substrates*, Langmuir, **26**, 12479, 2010.
11. S.F. CHINI, V. BERTOLA, A. AMIRFAZLI, *A methodology to determine the adhesion forces of arbitrarily shaped drops with convex contact lines*, Colloids and Surfaces A: Physicochemical and Engineering Aspects, **436**, 425–433, 2013.
12. V. BERTOLA, *Dynamic wetting of dilute polymer solutions: the case of impacting droplets*, Advances in Colloids and Interfaces, **193-194**, 1–11, 2013.
13. M.I. SMITH, V. BERTOLA, *Effect of polymer additives on the wetting of impacting droplets*, Physical Review Letters, **104**, 154502, 2010.
14. R. CROOKS, J. COOPER-WHITE, D.V. BOGER, *The role of dynamic surface tension and elasticity on the dynamics of drop impact*, Chemical Engineering Science, **56**, 5575–5592, 2001.
15. V. BERGERON, D. BONN, J.-Y. MARTIN, L. VOVELLE, *Controlling droplet deposition with polymer additives*, Nature, **405**, 772–775, 2000.
16. D. BAROLO, A. BOUDAUD, G. NARCY, D. BONN, *Dynamics of non-Newtonian droplets*, Phys. Rev. Lett., **99**, 174502, 2007.
17. J. VENZMER, *Superspreading – 20 years of physicochemical research*, Current Opinions in Colloid and Interface Science, **16**, 335–343, 2011.
18. N.P. CHEREMISINOFF, *Handbook of Engineering Polymeric Solutions*, Marcel Dekker, New York, 1997.
19. V.N. KALASHNIKOV, A.N. ASKAROV, *Relaxation time of elastic stresses in liquids with small additions of soluble polymers of high molecular weights*, Journal of Engineering Physics, **57**, 874–878, 1989.
20. J.E. GLASS, *Adsorption characteristics of water-soluble polymers. II poly(ethylene oxide) at the aqueous-air interface*, Journal of Physical Chemistry, **72**, 4459–4467, 1968.
21. V. BERTOLA, *An experimental study of bouncing Leidenfrost drops: comparison between Newtonian and viscoelastic liquids*, International Journal of Heat and Mass Transfer, **52**, 1786–1793, 2009.

22. M. REIN, *Phenomena of liquid-drop impact on solid and liquid surfaces*, Fluid Dynamic Research, **12**, 61–93, 1993.
23. V. BERTOLA, *The effect of polymer additives on the apparent dynamic contact angle of impacting drops*, Colloids and Surfaces A: Physicochemical and Engineering Aspects **363**, 135–140, 2010.
24. R.B. BIRD, P.J. DOTSON, N.L. JOHNSON, *Polymer solution rheology based on a finitely extensible bead-spring chain model*, Journal of Non-Newtonian Fluid Mechanics, **7**, 213–235, 1980.

Received April 19, 2015; revised version June 30, 2015.
